

ARTICLE

Open Access

PBK phosphorylates MSL1 to elicit epigenetic modulation of *CD276* in nasopharyngeal carcinoma

Meng-Yao Wang¹, Bin Qi¹, Fang Wang¹, Zhi-Rui Lin², Ming-Yi Li¹, Wen-Jing Yin¹, Yan-Yi Zhu¹, Lu He¹, Yi Yu¹, Fang Yang¹, Jin-Quan Liu¹ and Dong-Ping Chen¹

Abstract

CD276 (also known as B7–H3, an immune checkpoint molecule) is aberrantly overexpressed in many cancers. However, the upregulation mechanism and in particular, whether oncogenic signaling has a role, is unclear. Here we demonstrate that a pro-oncogenic kinase PBK, the expression of which is associated with immune infiltration in nasopharyngeal carcinoma (NPC), stimulates the expression of *CD276* epigenetically. Mechanistically, PBK phosphorylates MSL1 and enhances the interaction between MSL1 and MSL2, MSL3, and KAT8, the components of the MSL complex. As a consequence, PBK promotes the enrichment of MSL complex on *CD276* promoter, leading to the increased histone H4 K16 acetylation and the activation of *CD276* transcription. In addition, we show that *CD276* is highly upregulated and associated with immune infiltrating levels in NPC. Collectively, our findings describe a novel PBK/MSL1/*CD276* signaling axis, which may play an important role in immune evasion of NPC and may be targeted for cancer immunotherapy.

Introduction

Nasopharyngeal carcinoma (NPC) is one of the most common head and neck cancers in southeast Asia and north Africa^{1,2}. The standard treatment for patients with NPC is concurrent chemoradiation preceded or followed by systemic chemotherapy, according to the National Comprehensive Cancer Network (NCCN) guidelines. Although the local control rate has been significantly improved, approximately 30–40% of patients with locoregionally advanced NPC eventually develop distant metastasis after receiving radical treatment³. Novel strategies are alarmingly needed for NPC patients with a high risk of distant metastasis.

Evading immune destruction is described as the hallmark of cancer⁴. NPC originated from the epithelium of the nasopharyngeal, which is regarded as a highly immunogenic tumor characterized by heavy tumor-infiltrating lymphocytes (TILs), therefore at one time called “lymphoepithelial neoplasia”⁵. Furthermore, Epstein–Barr virus (EBV) infection is a major risk factor for the development of NPC in the endemic regions^{6,7}, upregulation of programmed cell death-ligand 1 (PDL1) was found in EBV-driven NPC cells, it is reported that PDL1 (*CD274*) expression on NPC is associated with a poor outcome⁸, this suggests that the development of NPC may be closely related to the immune escape of tumor cells. In pursuit of the novel effective treatment, several single-arm trials investigate that PD1 (*CD279*) inhibitors are effective in only 20–30% of recurrent or metastatic NPC patients^{9,10}, it is urgent to develop more biomarkers to reconstruct the immune surveillance, which would be exceedingly beneficial for the clinical intervention.


Correspondence: Jin-Quan Liu (liujinquan2018@163.com) or Dong-Ping Chen (dongpingchen_20@163.com)

¹Department of Radiation Oncology, Affiliated Cancer Hospital and Institute of Guangzhou Medical University, 510245 Guangzhou, China

²State Key Laboratory of Oncology in South China, Collaborative Innovation Center for Cancer Medicine, Sun Yat-Sen University Cancer Center, 510245 Guangzhou, China

These authors contributed equally: Meng-Yao Wang, Bin Qi, Fang Wang

© The Author(s) 2021, corrected publication 2021

 **Open Access** This article is licensed under a Creative Commons Attribution 4.0 International License, which permits use, sharing, adaptation, distribution and reproduction in any medium or format, as long as you give appropriate credit to the original author(s) and the source, provide a link to the Creative Commons license, and indicate if changes were made. The images or other third party material in this article are included in the article's Creative Commons license, unless indicated otherwise in a credit line to the material. If material is not included in the article's Creative Commons license and your intended use is not permitted by statutory regulation or exceeds the permitted use, you will need to obtain permission directly from the copyright holder. To view a copy of this license, visit <http://creativecommons.org/licenses/by/4.0/>.

CD276, also known as B7–H3, is a type I membrane protein with its sequence similarity to the extracellular domain of other B7 family members, which modulate T-cell function in a co-stimulatory or co-inhibitory manner^{11–13}. The CD276 protein is rarely expressed and is only found at low levels in normal human tissues^{14,15}. By contrast, recent studies found aberrant high CD276 expression on the many common malignancies, including stomach¹⁶, lung¹⁷, prostate¹⁸, kidney¹⁹, ovary²⁰, and endometrium²¹, and the high expression of CD276 was also correlated with advanced disease and poor outcome²². Moreover, CD276 protein is also frequently overexpressed on tumor vessels of human lung, breast, colon, endometrial, renal, and ovarian cancer, but not in the angiogenic vessels of the normal ovary¹⁵. Notably, an increasing number of studies support a pro-oncogenic role for CD276 in various human cancer types that is independent of its immune function^{15,23,24}. Overexpression of CD276 makes it an attractive target for the development of therapeutic agents, and in fact, CD276-targeting therapies are currently under clinical investigation in several children and adult tumors (NCT02982941, NCT01391143, NCT01099644, NCT02381314, and NCT04185038)^{15,25–31}. However, the cellular mechanisms that promote *CD276* expression are poorly understood.

A PDZ-binding kinase (PBK), also known as lymphokine-activated killer T-cell-originated protein kinase (TOPK), is a member of the novel MEK3/6-related mitogen-activated protein kinase–kinase (MAPKK) family³² and directly phosphorylates ERK, H2AX (Ser139), peroxiredoxin 1 (PRX1, Ser32), JNK1 (Thr183/Tyr185), and p53-related protein kinase (PRPK, Ser250)^{33–35}. Thus, PBK activates downstream signaling cascades via its phosphorylated substrates and plays an important role in many kinds of cellular processes, including growth, development, apoptosis, and inflammation³⁶. Previous studies including our group have highlighted that PBK was required for malignant phenotypes and was associated with poor prognosis of human common cancers, including NPC, oral cancer, breast cancer, colorectal cancer, leukemia and lymphoma, ovarian cancer, lung cancer, and glioma^{34,36–40}. Due to the broad expression of PBK across multiple tumor types, specific inhibitors have been developed to target PBK, including HI-TOPK-032⁴¹, OTS514/OTS964⁴², and ADA-07⁴³, and show high therapeutic potency in the preclinical study. PBK has been revealed to contribute to the regulation of proliferation and cell cycle progression, whereas whether PBK involves in the tumor immune evasion is not reported so far. In the current study, we revealed that PBK promotes the transcription of *CD276* via an epigenetic way, providing new insight into immune evasion in NPC.

Results

PBK expression is associated with immune infiltration

The level of TILs is an independent predictor of sentinel lymph node status and survival in many cancers including NPC⁴⁴. To explore the role of *PBK* in immune regulation of NPC, we investigated whether *PBK* expression was correlated with immune infiltration levels in NPC. ImmuCellAI⁴⁵, a highly accurate method, was used to estimate the infiltration abundance of immune cells from RNA-seq expression profiles of two NPC cohorts (GSE102349 and GSE68799). Interestingly, correlation analysis showed that *PBK* expression was significantly correlated to the infiltration of neutrophil and monocyte cells (Fig. 1a), which were reported to promote the immune evasion of tumors^{46–48}, but negatively correlated to the infiltration of natural killer (NK) and B cells (Fig. 1b), which were reported to repress the immune evasion of tumors^{49–51}. Moreover, ImmuCellAI was designed to estimate the abundance of 18 T-cell subsets that are major players in the tumor microenvironment. Notably, *PBK* expression has significant correlations with CD8-naive cell, nTreg cell, and Th2 cell (Fig. 1c), but was negatively correlated to the infiltration of Tfh cell, CD4+ T cell, and Th17 cell (Fig. 1d). Based on these results, it is supposed that high *PBK* expression is closely associated with compromised immune microenvironment in NPC.

PBK regulates the transcription of *CD276*

Given the pivotal roles of T-cell subsets in cancer initiation, progression, and immunotherapy^{52–54}, we focus on how PBK modulates the infiltration of T-cell subsets. Accumulating evidence has indicated that cancer cells could upregulate a series of immune inhibitory factors to repress the proliferation, cytokine production, and effector activities of T cells, in turn leading to immune evasion^{55–57}. Thus, we investigated whether previously reported immune inhibitory molecules of T cells, including *PDL1* (*CD274*), *PDL2* (*CD273*), *CD276*, *IL10*, and *IDO1*, could be downstream targets of PBK. The results of quantitative polymerase chain reaction (qPCR) showed that only *CD276* was significantly downregulated in CNE2 cells after PBK knockdown by siRNA in our primary screening (Fig. 2a and Fig. S1). Further, qPCR and immunoblotting assays revealed that the mRNA and protein level of *CD276* were downregulated in CNE2 and SUNE1 cells with PBK depletion by two siRNAs (Fig. 2b and Fig. S2a), but were upregulated in HK1 and CNE1 cells with PBK overexpression (Fig. 2c and Fig. S2b), suggesting that *CD276* is a bona fide downstream target of PBK.

To investigate whether the PBK kinase activity is indispensable for the regulation of *CD276*, we treated CNE2 and SUNE1 cells with OTS514, a PBK kinase-specific inhibitor^{58,59}, followed by qPCR and immunoblotting

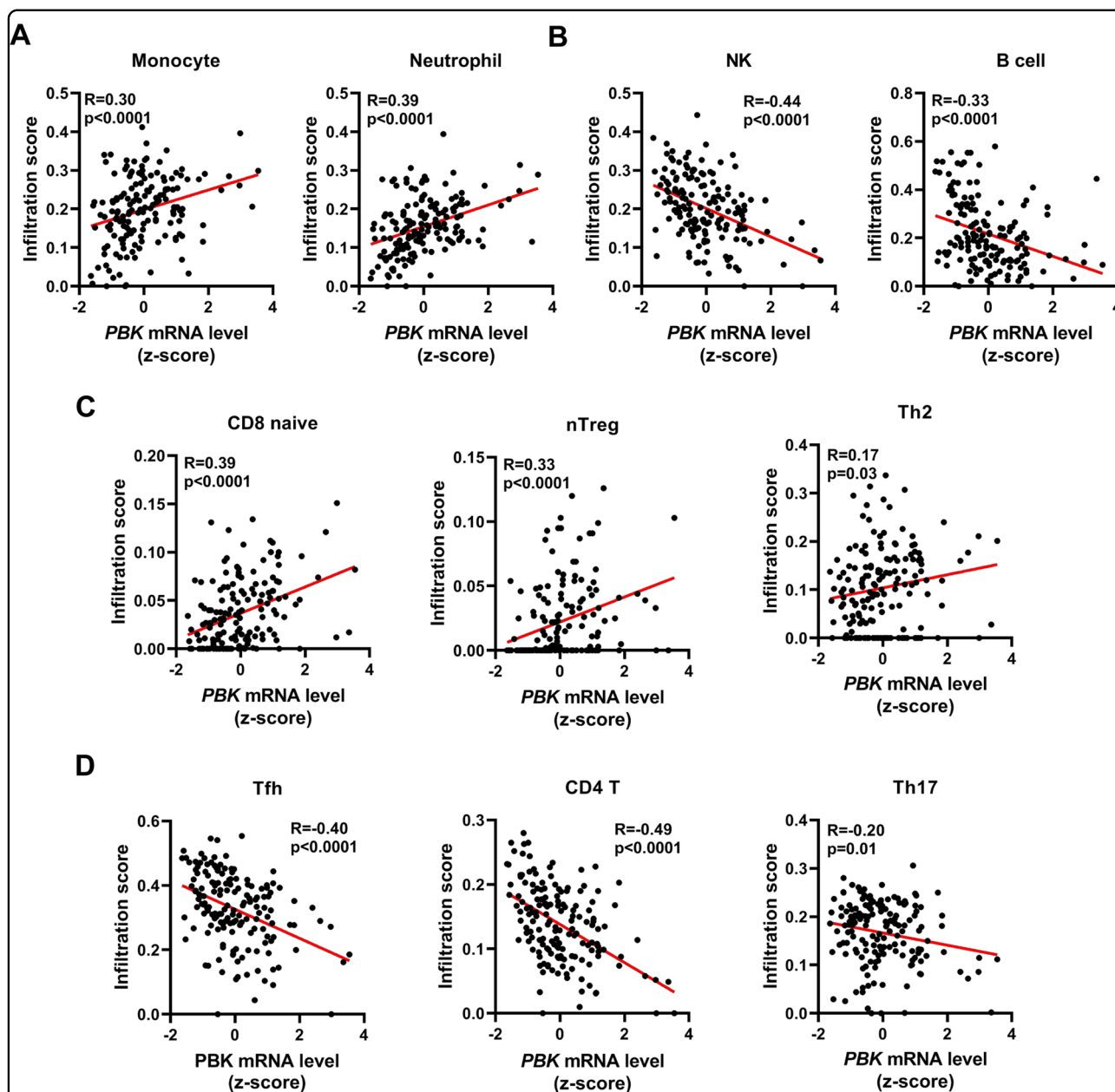


Fig. 1 *PBK* mRNA level is associated with immune cell infiltration. **A** The scatterplots show that the mRNA level of *PBK* (lymphokine-activated killer T-cell-originated protein kinase) is significantly correlated with the infiltration of neutrophil cells (left), monocyte cells in NPC (nasopharyngeal carcinoma). **B** The scatterplots show that the mRNA level of *PBK* is negatively correlated with the infiltration of NK (natural killer) cells (left) and B cells in NPC. **C** The scatterplots show that the mRNA level of *PBK* is significantly correlated with the infiltration of CD8-naive cell (left), nTreg cell (middle), and Th2 cell. **D** The scatterplots show that the mRNA level of *PBK* is negatively correlated with the infiltration of Tfh cell (left), CD4+ T cell (middle), and Th17 cell. The method called ImmuCellAI was used to estimate the abundance of 24 immune cell types from two integrated NPC RNA-seq data (GSE102349, GSE68799). A Pearson correlation test was used (two-tailed) ($n = 159$).

assays, and found that compared to DMSO treatment, OTS514 treatment decreased the mRNA and protein level of CD276 in a dose-dependent manner (Fig. 2d and Fig. S2c). According to previous reports³⁹, we construct two *PBK* mutants, including kinase-active mutants (*PBK*-

T198E) and kinase-dead mutants (*PBK*-T198A). Both qPCR and immunoblotting assays revealed that *PBK*-WT and *PBK*-T198E but not *PBK*-T198A could rescue the repression of *CD276* mediated by a *PBK* siRNA that targets the 3'UTR region (Fig. 2e and Fig. S2d). These data

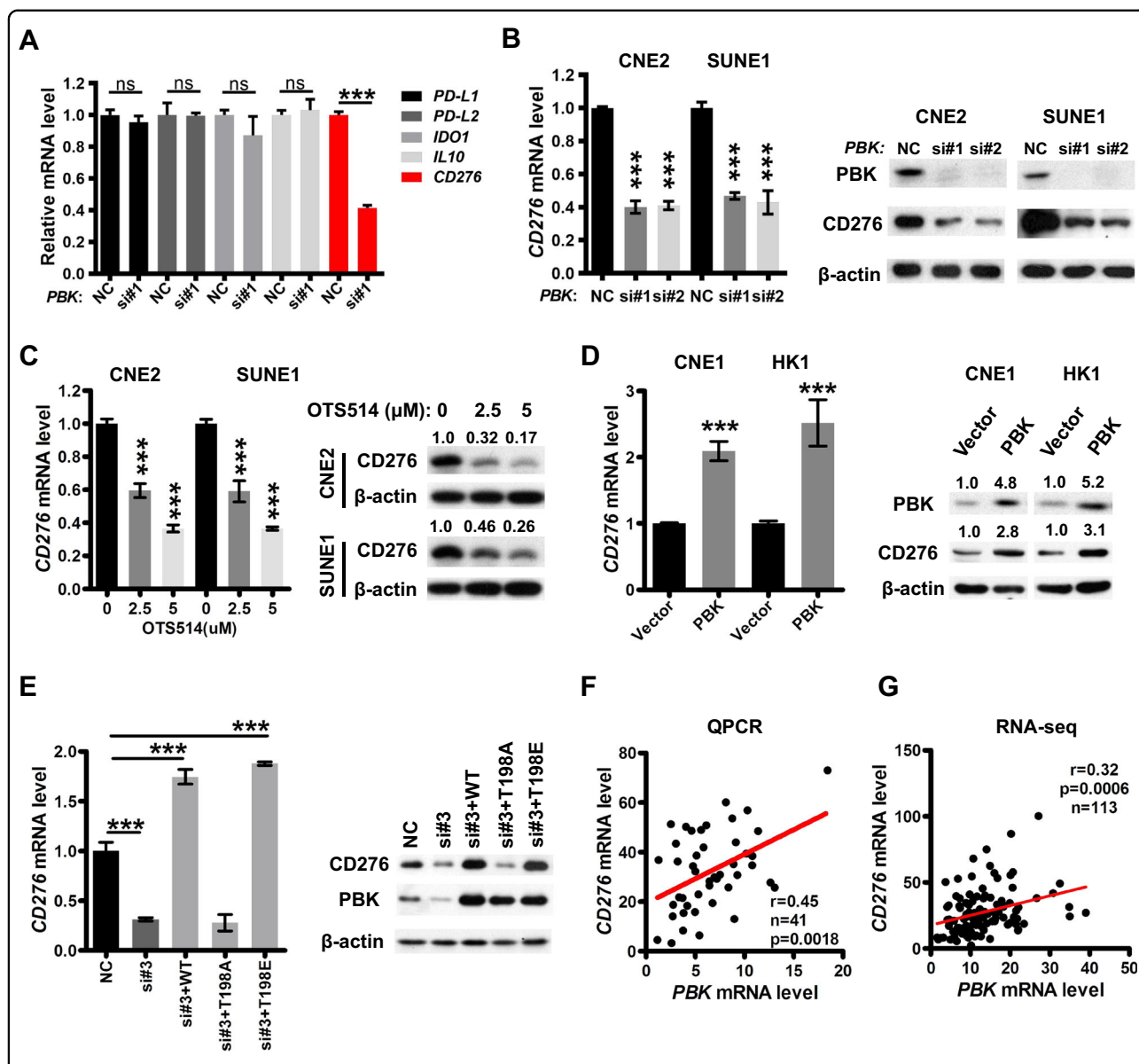


Fig. 2 PBK regulates the transcription of *CD276* dependent on its kinase activity. **A** CNE2 cells were transfected with one *PBK* siRNA or NC (nonspecific siRNA) for 48 h and qPCR (quantitative polymerase chain reaction) was performed to measure the mRNA expression of indicated genes. **B** CNE2 and SUNE1 cells were transfected with two *PBK* siRNAs or NC (nonspecific siRNA) for 48 h. qPCR and immunoblotting were conducted to measure the mRNA and protein expression of *CD276*. Left, qPCR. Right, immunoblotting with indicated antibodies. **C** CNE2 and SUNE1 cells were treated with DMSO (dimethylsulfoxide) or OTS514 (2.5 and 5 μM) for 24 h. qPCR and immunoblotting were conducted to measure the mRNA and protein expression of *CD276*. Left, qPCR. Right, immunoblotting with indicated antibodies. **D** CNE1 and HK1 cells were infected by lentiviruses carrying *PBK* coding region to establish the *PBK*-overexpression stable cell lines. qPCR and immunoblotting were conducted to measure the mRNA and protein expression of *CD276*. Left, qPCR. Right, immunoblotting with indicated antibodies. **E** CNE2 and SUNE1 cells were transfected with one siRNA targeting *PBK* 3'UTR (untranslated region) or NC (nonspecific siRNA). After 24 h, the cells were transfected with *PBK* constructs, including WT (wild type), kinase-dead (T198A), or kinase consistently activated (T198E) for another 24 h. qPCR and immunoblotting were conducted to measure the mRNA and protein expression of *CD276*. Left, qPCR. Right, immunoblotting with indicated antibodies. **A–E** In qPCR assays, *ACTB* was used as the loading control, and the mRNA level of indicated genes is normalized to *ACTB*. The results are shown as the fold change over NC (nonspecific siRNA). Data present as the mean ± SEM (standard error of the mean) ($n = 3$). *** $P < 0.001$ (student's *t* test for two groups, one-way ANOVA for three groups). All the experiments were performed independently three times with similar results, and the data are representative of three independent experiments. **F–G** Correlation analyses between the *PBK* and *CD276* mRNA level were performed using our qPCR data (**F**) or public RNA-seq data (**G**). A Pearson correlation test was used (two-tailed).

show that PBK regulates *CD276* transcription dependent on its kinase activity.

Furthermore, correlation analysis showed that the mRNA expression of *PBK* and *CD276* is positively correlated in our NPC cohort detected by qPCR ($r = 0.45$, $n = 41$, $p = 0.0018$, Fig. 2f) as well as in the NPC RNA-seq dataset ($r = 0.32$, $n = 113$, $p = 0.0006$, Fig. 2g). Notably, pan-cancer correlation analysis between *PBK* and *CD276* was conducted using the mRNA expression data from TCGA. The result reveals that the mRNA level of *PBK* is positively correlated with *CD276* in several common cancers (Fig. S3), including adrenocortical carcinoma, brain lower-grade glioma, kidney renal clear-cell carcinoma, kidney renal papillary cell carcinoma, liver hepatocellular carcinoma, lung adenocarcinoma, pancreatic adenocarcinoma, prostate adenocarcinoma, and thyroid carcinoma, indicating that this is a general mechanistic upregulation of *CD276* by PBK in cancers.

PBK regulates *CD276* transcription dependent on MSL1

Considering that PBK is a kinase, not a transcription regulator, there is a mediator involved in *CD276* transcription regulation by PBK. In order to identify the mediator, we carried out immunoprecipitation and mass spectrometry analysis and identified MSL1 as an interacting partner of PBK (Fig. 3a). Co-immunoprecipitation assays validated the exogenous interaction between PBK and MSL1 in 293T cells (Fig. 3b). To further confirm the *in vivo* interaction, total proteins from CNE2 and SUNE1 cells were extracted, and immunoprecipitation was performed with an antibody against PBK followed by immunoblotting with an antibody against MSL1, demonstrating that MSL1 was efficiently co-immunoprecipitated with PBK (Fig. 3c). Since PBK has serine/threonine kinase activity, we investigated whether MSL1 is a phosphorylation target of PBK. Immunoprecipitation assays using an antibody against phosphorylated serine/threonine followed by immunoblotting analysis using MSL1 antibody demonstrated that the phosphorylation level of MSL1 was enhanced in PBK-overexpression cells (Fig. 3d and Fig. S4a), but was decreased in PBK-knockdown cells (Fig. 3e and Fig. S4b) as well as in cells treated with PBK inhibitor (Fig. 3f and Fig. S4c). These data show that PBK indeed interacts with and phosphorylates MSL1.

Furthermore, qPCR and immunoblotting results showed that MSL1 depletion decreased the expression of *CD276* (Fig. 3g and Fig. S4d) and MSL1 overexpression increased the expression of *CD276* (Fig. 3h and Fig. S4e), suggesting that MSL1 is involved in the transcriptional regulation of *CD276*. More importantly, the knockdown of MSL1 repressed the upregulation of *CD276* mediated by PBK overexpression (Fig. 3i and Fig. S4f). MSL1 contains multiple serine/threonine residues, six of which (Ser66, Ser126, Ser205, Ser393, Thr396, and Ser442) were

reported as phosphorylation sites^{60,61}. Given that the target sites of MSL1 phosphorylated by PBK are unknown, we replaced all of those MSL1 serine/threonine residues noted above individually with an alanine residue (S/T > A-MSL1). The result of qPCR showed that MSL1 wild-type but not MSL1-S/T > A mutant overexpression could rescue the downregulation of *CD276* after PBK depletion in CNE2 and SUNE1 cells (Fig. 3j and Fig. S4g), indicating that PBK controls the transcription of *CD276* dependent on the phosphorylation status of MSL1.

PBK promotes the enrichment of MSL complex on *CD276* promoter

MSL1 acts as a scaffold to tether MSL2, MSL3, and KAT8 (MOF) together for the formation of the MSL histone acetyltransferase complex, in turn leading to histone H4 Lys16 acetylation (forming H4K16ac), thereby efficiently increasing the gene expression^{62,63}. Apart from the dosage-compensation role of the MSL complex, accumulating evidence suggests that MSL proteins may be involved in additional functions, such as transcription regulation^{64–67}. To address the role of PBK in the MSL complex, we conducted immunoprecipitation experiments using an antibody against MSL1 followed by immunoblotting with antibodies against the components of the MSL complex in PBK-overexpression or PBK-knockdown cells, respectively. The results demonstrated that PBK overexpression could enhance the physical association between MSL1 and MSL2, MSL3, and KAT8 (Fig. 4a and Fig. S5a), whereas PBK depletion obviously inhibited these interactions (Fig. 4b and Fig. S5b). Moreover, quantitative chromatin immunoprecipitation (qChIP) analysis using specific antibodies against MSL1 or KAT8 showed that the occupancy of MSL1 and KAT8 on the *CD276* promoter region is increased in PBK-overexpression cells (Fig. 4c) but decreased in PBK-deficient cells (Fig. 4d). Consistently, the acetylation level of histone H4 Lys16 on the promoter region is increased in PBK-overexpression cells but decreased in PBK-deficient cells, as indicated by qChIP results (Fig. 4e, f).

High expression of *CD276* is associated with the immune infiltration in NPC

Since the role of *CD276* in NPC remains unknown, we performed a qPCR assay and found that *CD276* mRNA expression in NPC tissues was higher than in the non-cancerous NP tissues (Fig. 5a). In addition, in agreement with our qPCR result, gene expression profiles derived from the GEO (GDS3341, GSE40290, and GSE53819⁶⁸) showed that compared to noncancerous NP tissues, the *CD276* mRNA level was obviously elevated in the NPC tissues (Fig. 5b). Previous reports showed that *CD276* has been associated with co-stimulatory as well as co-inhibitory functions in regulating T-cell responses^{12,14,69,70}. In NPC, correlation

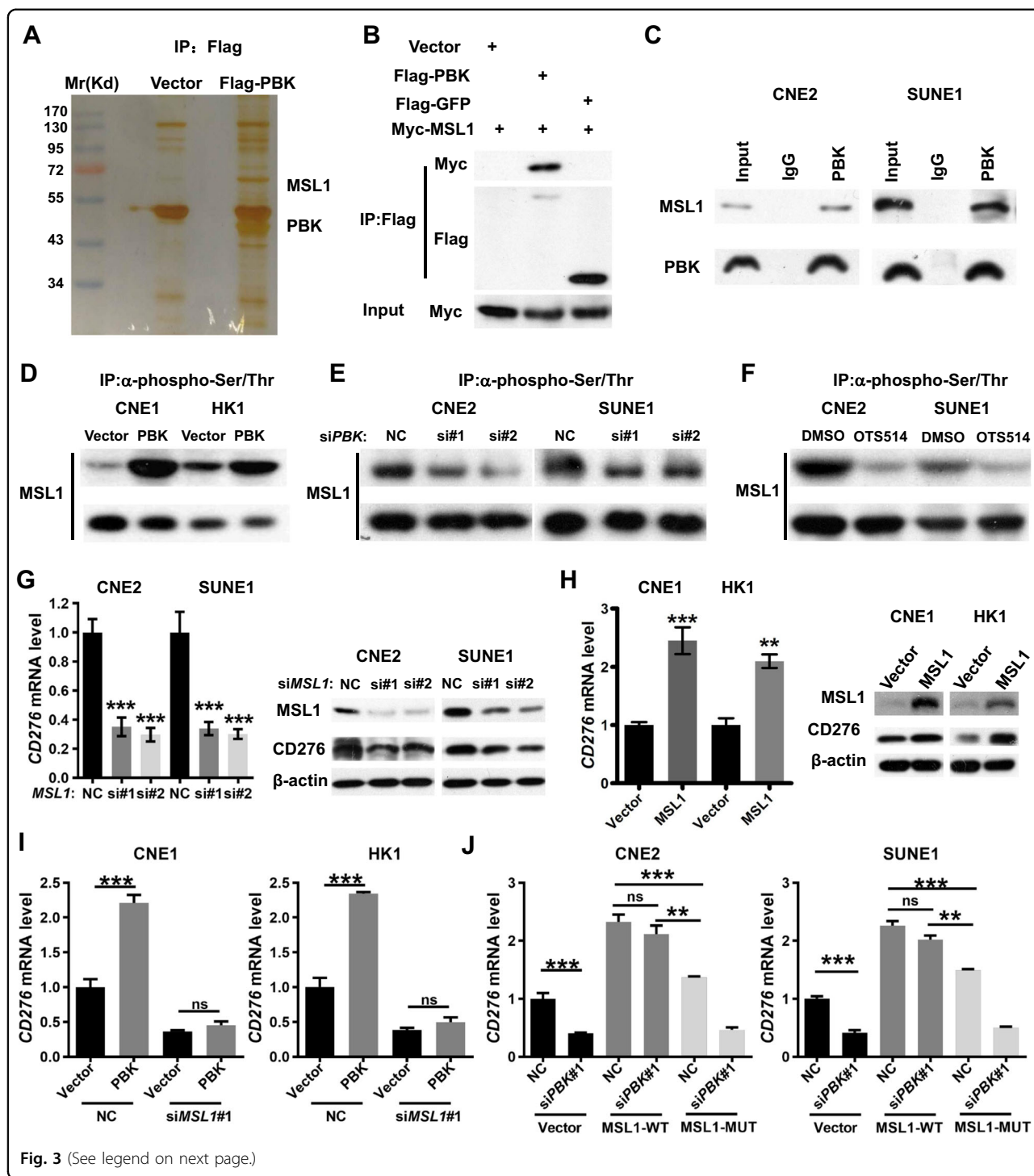


Fig. 3 (See legend on next page.)

analysis showed that *CD276* mRNA level was positively associated with the infiltration level of CD8-naive cell, nTreg cell, and Th2 cell (Fig. 5c), but was negatively associated with the infiltration level of CD4 T cell, Tfh cell, and Th1 cell (Fig. 5d). In addition, *CD276* expression has a

significant correlation with monocyte and neutrophil cells and a negative correlation with NK and B cells (Fig. 5e). Taken together, our findings demonstrated that *CD276* is upregulated in NPC and associated with immune cell infiltration.

(see figure on previous page)

Fig. 3 PBK regulates the expression of CD276 dependent on MSL1. **A** SDS/PAGE and silver staining analysis of proteins pulled down by Flag-PBK or vector, via anti-Flag affinity purification. Mass spectrometry analysis recognized MSL1 (male-specific lethal 1 homolog) as an interacting partner of PBK. **B** 293T cells were co-transfected Myc-MSL1 with vector, Flag-GFP (green fluorescent protein), or Flag-PBK for 36 h, and immunoprecipitation assays and immunoblotting analyses with the indicated antibodies were performed. **C** Endogenous immunoprecipitation assay in CNE2 and SUNE1 cells with an anti-PBK antibody followed by immunoblotting with antibodies against the indicated proteins. **D** Immunoprecipitation assays and immunoblotting analyses with the indicated antibodies were performed in PBK-overexpression stable cell lines or control cell lines. **E** CNE2 and SUNE1 cells were transfected with *PBK* siRNAs or NC (nonspecific siRNA) for 48 h. Immunoprecipitation assays and immunoblotting analyses with the indicated antibodies were performed. **F** CNE2 and SUNE1 cells were treated with DMSO or OTS514 (5 μ M) for 24 h. Immunoprecipitation assays and immunoblotting analyses with the indicated antibodies were performed. **G** CNE2 and SUNE1 cells were transfected with two *MSL1* siRNAs or NC (nonspecific siRNA) for 48 h. qPCR and Immunoblotting were conducted to measure the mRNA and protein expression of *CD276*. Left, qPCR. Right, immunoblotting with indicated antibodies. **H** CNE1 and HK1 cells were infected by lentiviruses carrying *MSL1* coding region to establish the *MSL1* overexpression stable cell lines. qPCR and immunoblotting were conducted to measure the mRNA and protein expression of *CD276*. Left, qPCR. Right, immunoblotting with indicated antibodies. **I** PBK-overexpression cell lines or control cell lines were transfected with one *MSL1* siRNA or NC (nonspecific siRNA) for 48 h, respectively. qPCR assays were conducted to measure the mRNA level of *CD276*. Left, CNE1 cell lines, right, HK1 cell lines. **J** *MSL1* wild type or serine/threonine residues' mutant overexpression cell lines or control cell lines were transfected with a *PBK* siRNA or NC (nonspecific siRNA) for 48 h. qPCR assays were conducted to measure the mRNA level of *CD276*. Left, CNE2 cell lines, right, SUNE1 cell lines. **J** In qPCR assays, *ACTB* was used as the loading control, and the mRNA level of *CD276* is normalized to *ACTB*. The results are shown as the fold change over NC (nonspecific siRNA). Data present as the mean \pm SEM ($n = 3$). $^{**}P < 0.01$, $^{***}P < 0.001$, ns not significant (Student's *t* test for two groups, one-way ANOVA for three groups). All the experiments were performed independently three times with similar results and the data are representative of three independent experiments.

PBK reduces T-cell-mediated cytotoxicity dependent on CD276

In order to investigate whether the PBK/CD276 axis plays an important role in tumor immune evasion, we conducted the cytotoxic T-lymphocyte assay. Since the NPC cell lines used above did not express HLA-A2 that is important for tumor cell recognition by HLA-A2+ T cells, we selected another NPC cell line TW03 with HLA-A2 positive for the cytotoxic T-lymphocyte assay. The results showed that PBK knockdown significantly increased the percentage of lysis TW03 cells when the tumor cells were cocultured with CD3/CD28-activated human HLA-A2+ T lymphocytes, and this increase was markedly reversed by the recovery of CD276 (Fig. 6A). On the other hand, PBK overexpression significantly reduced the percentage of dead TW03 cells, and this decrease was markedly rescued by *CD276* knockdown (Fig. 6B). Collectively, these data confirm that PBK contributes to the limitation of T-lymphocyte attack on NPC cells dependent on CD276.

Discussion

Herein, our findings provide new insight into understanding the potential role of PBK in tumor immunology. We demonstrate that *PBK* expression is correlated with infiltration levels of diverse immune cells in NPC. Specifically, the infiltration levels of tumor-promoting leukocytes, including neutrophil, monocyte, CD8-naive, nTreg, and Th2 cells, were positively correlated with *PBK* mRNA expression. Simultaneously, the infiltration levels of tumor-repressing leukocytes, including NK, B, Tfh, CD4+ T cells, and Th17, were negatively correlated with *PBK* mRNA expression. These correlation patterns are at least partly attributed to the transcription regulation of the

CD276 gene by PBK. Although the role of CD276 in antitumor immunity has been controversial with conflicting co-stimulatory and co-inhibitory functions, CD276 may exert a protumor effect on tumor progression in NPC based on the results that the expression of *CD276* is much higher in tumor samples than normal samples and is associated with the compromised immune micro-environment. Since several immunomodulatory agents, especially anti-PD1 and anti-PDL1 antibodies, have shown great promise in treating advanced NPC, the role of the PBK/CD276 axis in immunotherapy response is further to be elucidated.

PBK, a dual-specificity serine/threonine kinase, plays an important role in the activation of the Raf/MEK/ERK pathway to promote cell proliferation, colony formation, and cancer development. For example, PBK facilitates transformation by upregulating and activating ERK2 through an increase in AP-1 (c-Jun) transcriptional activity and increased tumorigenesis of HCT116 colorectal cancer^{33,71}. PBK can also directly bind to and phosphorylate AP-1 (c-Jun) after solar ultraviolet exposure^{72,73}. Besides a potential central player of the MAPK cascade mechanism, PBK binds with other proteins and promotes various cancer-related processes, such as PBK promotes tumor dissemination by direct phosphorylation of p53-related protein kinase (PRPK)⁷⁴. PBK regulates autophagy by phosphorylating ULK1 and promotes glioma resistance to TMZ (temozolomide)⁷⁵. Thus, more research is necessary to identify potential downstream targets of PBK. Herein, we identify MSL1 as a previous unknown substrate of PBK. Indeed, PBK phosphorylates MSL1 and promotes the formation of the MSL complex. However, the specific phosphorylation site(s) of MSL1 and target genes of the PBK/MSL1 axis are needed to be explored.

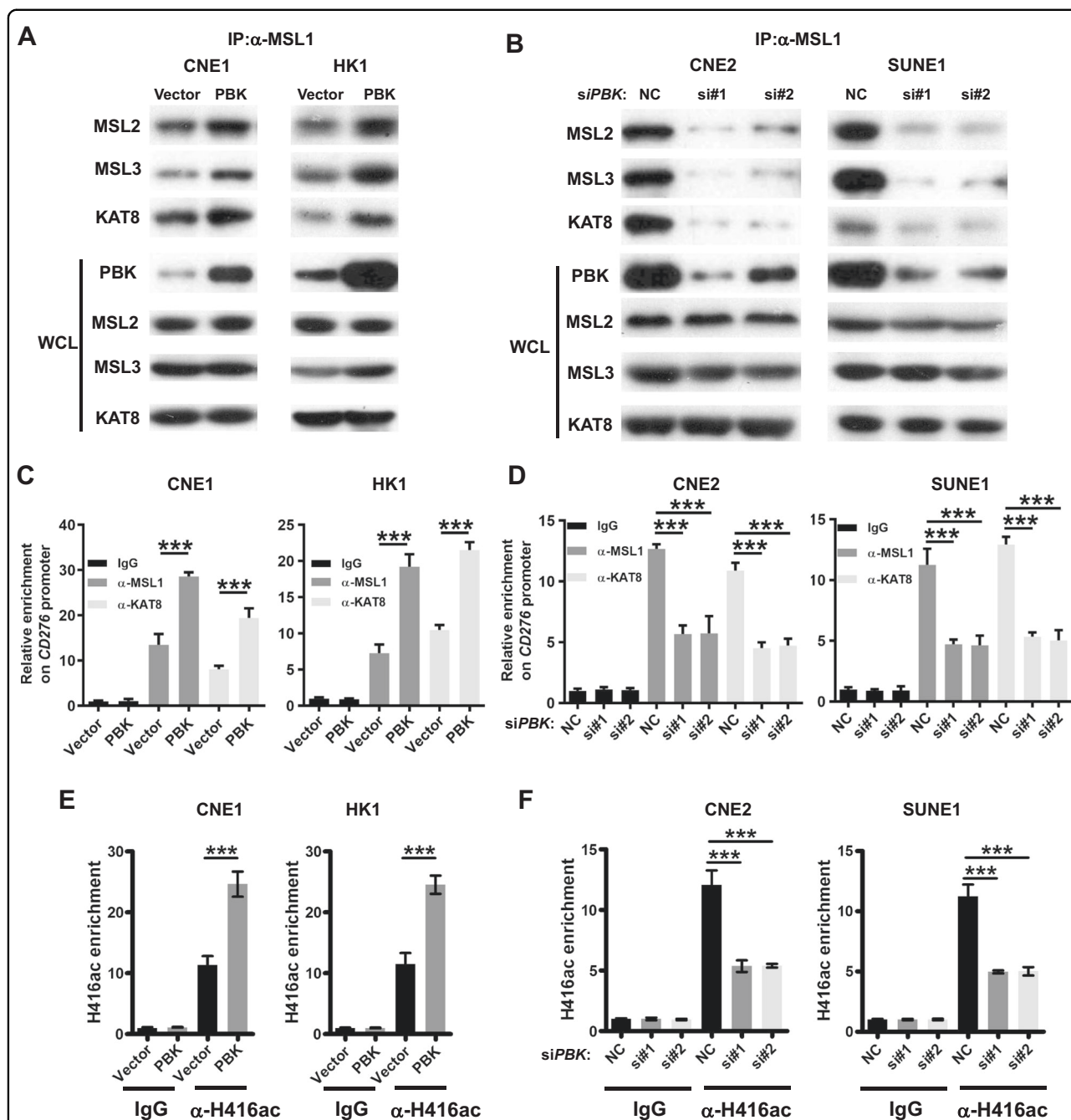


Fig. 4 PBK promotes the formation of MSL complex on the promoter of CD276. **A** Immunoprecipitation assays with MSL1 antibody and immunoblotting analyses with the indicated antibodies were performed in PBK-overexpression stable cell lines. Left, CNE1, right, HK1. **B** CNE2 and SUNE1 cells were transfected with *PBK* siRNAs or NC (nonspecific siRNA) for 48 h. Immunoprecipitation assays with MSL1 antibody and immunoblotting analyses with the indicated antibodies were performed. Left, CNE2, right, SUNE1. **C** ChIP-qPCR (chromatin immunoprecipitation-quantitative PCR) analysis of *CD276* promoter using antibodies against MSL1 and KAT8 in PBK-overexpression or control cell lines. Left, CNE1, right, HK1. **D** ChIP-qPCR analysis of *CD276* promoter using antibodies against MSL1 and MOF in PBK-knockdown or control cells. Left, CNE2, right, SUNE1. **E**, **F** ChIP-qPCR analysis of *CD276* promoter using antibodies against H4K16ac (acetylation of histone H4 on lysine 16) in PBK-overexpression (**E**) or -knockdown cells (**F**). In **C–F**, ChIP-qPCR results were presented as the fold change over the vector/IgG or NC/IgG group. Error bars represent the mean ± SD (standard deviation) for three biological replicates. ****P* < 0.001 (student's *t* test for two groups, one-way ANOVA for three groups). All the experiments were performed independently three times with similar results and the data are representative of three independent experiments.

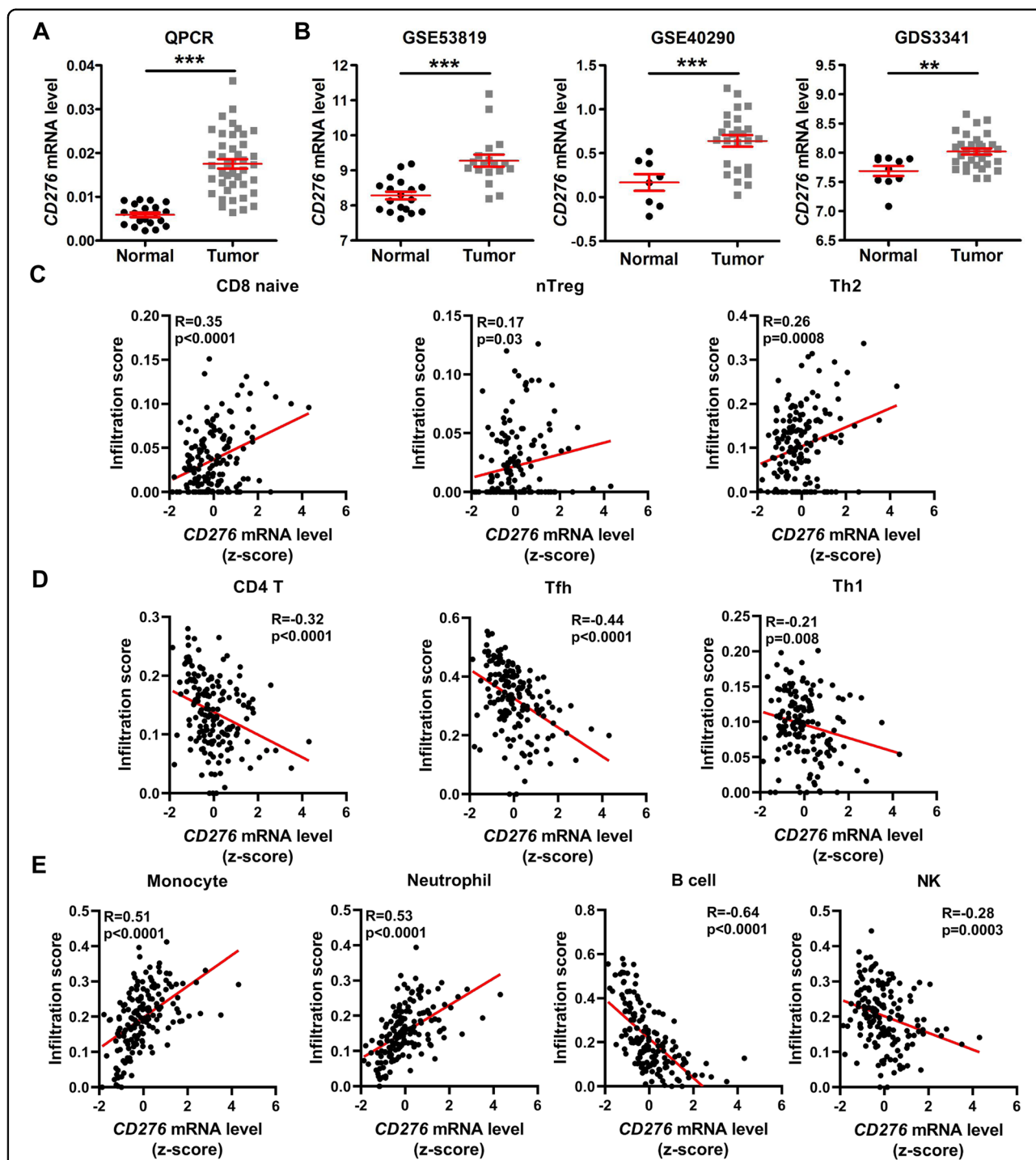
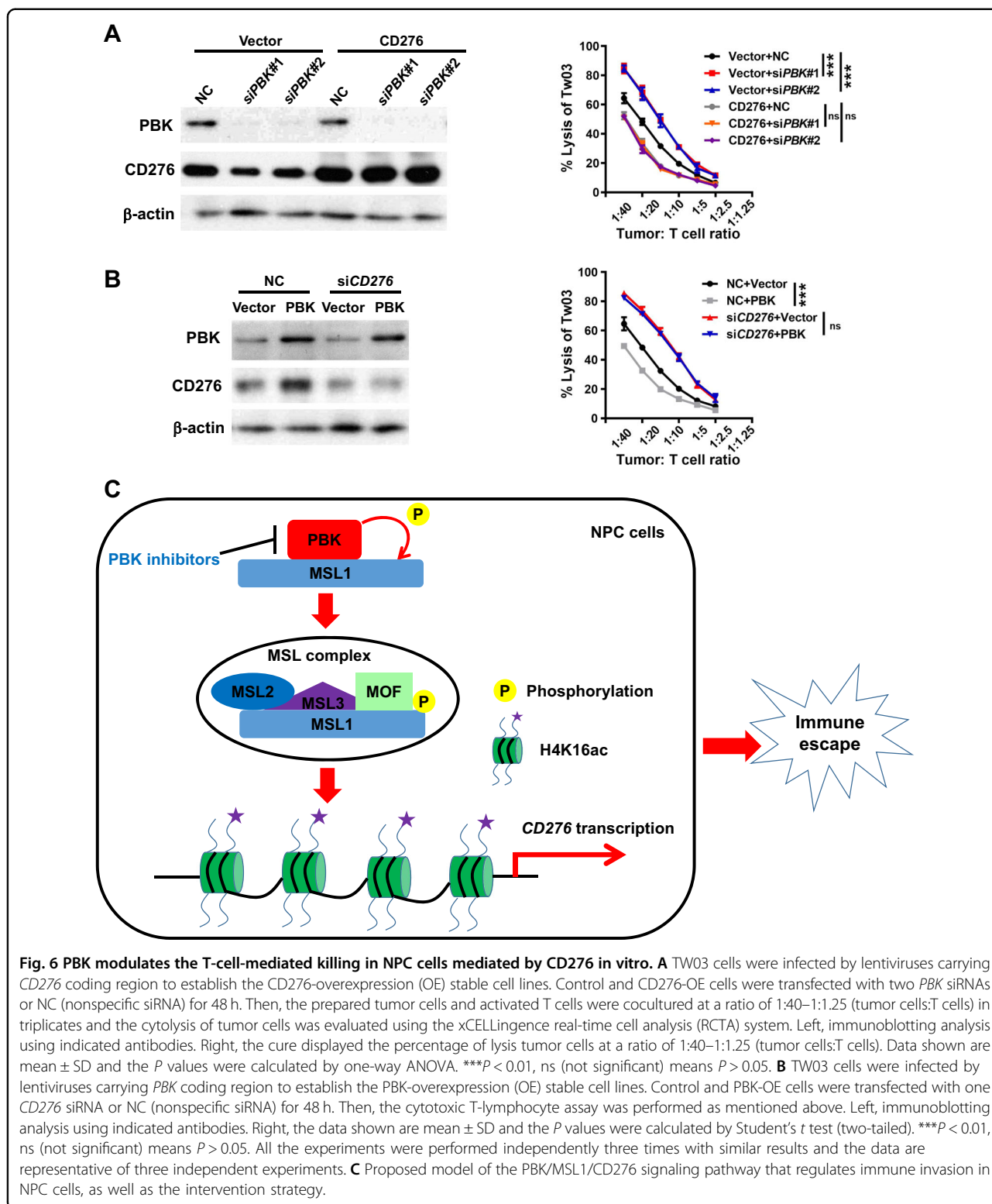


Fig. 5 *CD276* is upregulated and associated with immune infiltration in NPC. **A** The graphs show that *CD276* is significantly upregulated in NPC samples ($n = 41$) compared to normal samples ($n = 20$) via qPCR analysis. $***p < 0.001$ was determined by Student's t test. **B** The graphs show that *CD276* is significantly upregulated in NPC samples compared to normal samples, as indicated by four public datasets from GEO (Gene Expression Omnibus database). $**p < 0.01$, $***p < 0.001$ was determined by Student's t test. **C** Correlation analysis between the *CD276* mRNA level and the tumor-promotion T-cell subset infiltration, including CD8-naive cell (left), nTreg cell (middle), and Th2 cell using publicly available NPC RNA-seq data. A Pearson correlation test was used (two-tailed). **D** Correlation analysis between the *CD276* mRNA level and the tumor-repression T-cell subset infiltration, including CD4 T cell (left), Tfh cell (middle), and Th1 cell using publicly available NPC RNA-seq data. A Pearson correlation test was used (two-tailed). **E** Correlation analysis between the *CD276* mRNA level and the infiltration level of monocyte, neutrophil, NK, and B cells using publicly available NPC RNA-seq data. A Pearson correlation test was used (two-tailed).



CD276 mRNA is widely expressed in many tissues and notably aberrantly expressed in various types of cancer. However, compared to *PDL1*, the cellular mechanisms that regulate *CD276* expression in cancer cells are poorly

understood. So far, only a few findings identified revealed that overexpression of *CD276* in tumor tissues was highly correlated with decreased expression of several miRNAs as compared to normal tissues, suggesting that a

microRNA regulatory mechanism is involved in its differential expression^{76,77}. In this report, we first present an epigenetic modulation mechanism of *CD276* expression. Specifically, PBK phosphorylates MSL1 and promotes the enrichment of MSL complex on the promoter region of *CD276*, in turn leading to an increase in histone H4 Lys16 acetylation, thereby activating the transcription of *CD276* and suppressing the cytotoxic T-cell function (Fig. 6C). Further investigations need to be conducted to clarify which transcription factors are essential for *CD276* transcription.

In summary, what is noteworthy is that this is the first demonstration of PBK modulation of a co-inhibitory signal *CD276* induction to escape from immunosurveillance in NPC. Our results highlight the potential clinical benefits of targeting both PBK and *CD276* in NPC patients with a high risk of progression.

Materials and methods

Cell culture

The 293T cells and the human NPC cell lines, including CNE2, SUNE1, HK1, and CNE1, were maintained in Dulbecco's modified Eagle's medium supplemented with 10% FBS at 37 °C and 5% CO₂. All the cell lines were tested for negative mycoplasma contamination.

Sample collection

Fresh frozen tissues for qPCR analysis were resected from histopathologically and clinically diagnosed NPC patients. All samples were obtained from the tumor resource bank of Guangzhou Medical University Affiliated Cancer Hospital and Institute. All patients supplied informed consent.

Plasmids and mutagenesis

Full-length human PBK cDNA was amplified and cloned into a pcDNA6B-his-myc vector (ECORI and XhoI) or plenti-puro vector (ECORI and XhoI). Full-length human MSL1 cDNA was amplified and cloned into pCMV-N-flag (BamHI and ECORI). ClonExpress II One Step Cloning Kit (Vazyme) was used according to the manufacturer's instructions.

pcDNA6B-his-myc-PBK(T198A), pcDNA6B-his-myc-PBK(T198E), and pCMV-N-flag-MSL1(S/T > A) mutants were constructed using a QuikChange site-directed mutagenesis kit (Stratagene) according to the manufacturer's instructions. Sequences of the constructs were all verified by Sanger sequencing.

The primers used are listed as follows:

1. PBK with pcDNA6B-his-myc vector:
forward: 5'-TAGTCCAGTGTGGTGGGAATTCATGGAAGGGATCAGTAATTTCAAGA-3'
reverse: 5'-CGCGGGCCCTCTAGACTCGGACATCTGTTTCCAGAGCTT-3'

2. PBK with plenti-puro vector:
forward: 5'-CTACCGGACTCAGATCTCGAGATGGAAGGGATCAGTAATTTCAAGA-3'

reverse: 5'-GTCATCCTTGTAATCGAATTCGACATCTGTTTCCAGAGCTTCAACA-3'

3. MSL1 with pCMV-N-flag:
forward: 5'-GATAAGAGCCCGGGCGGATCCATGGAAGGCGGATGCAGC-3'

reverse: 5'-TCTGTCGACGATATCGAATTCCTATTTCTACACGTCCGGTGAG-3'

PBK inhibitor

The PBK inhibitor OTS514 was purchased from Selleck (S7652) and dissolved in DMSO with a stocked concentration (50 mM). For the functional assays, NPC cell lines CNE2 and SUNE1 were treated with the OTS514 at two different concentrations, including 2.5 and 5 μM.

siRNA transfection

The specific siRNAs and control nonspecific siRNA (NC) were obtained from Guangzhou RiboBio Co., Ltd. Cancer cells were counted and seeded into 6-well plates with 2 × 10⁵ cells/well. After 24 h, the cells were 30–40% confluent and transfected with siRNAs using RNAiMAX transfection reagents (Invitrogen) according to the manufacturer's instructions. The cells were harvested for further experiments after 24 or 48 h. The siRNA targeting sequences were as follows:

siPBK#1: 5'-GAATATGGCAAGAGGGTTAAA-3'

siPBK#2: 5'-GGGAACTAGGCCACCTATTAA-3'

siPBK#3: 5'-GAAGTGTGGCTTGCGTAAATA-3'

siMSL1#1: 5'-CACCGGACGTGTAGGAAATAG-3'

siMSL1#1: 5'-ATGTTATCACTCGCTGATAAT-3'

siCD276: 5'-AAAGAAGATGATGGACAAG-3'.

RNA extraction and qPCR

Total RNA was extracted using the TRIzol Reagent (Invitrogen) according to the manufacturer's instructions. Reverse transcription was performed using a cDNA Synthesis Kit (Thermo, K1622). The quantitative real-time polymerase chain reaction was conducted using ChamQ SYBR Color qPCR Master Mix (Vazyme, Q411-02). The sequences of the PCR primers used for amplification were as follows:

ACTB forward, 5'-AAGGTCATCC CTGAGCT GA A-3'

ACTB reverse, 5'-TGACAAAGTG GTCGTTG AGG-3'

PBK forward, 5'-GCGGTGAGACTCTGGACTGA-3'

PBK reverse, 5'-CTGCATAAACGGAGAGGCCG-3'

CD276 forward, 5'-GGAGAATGCAGGAGCTGAG G-3'

CD276 reverse, 5'-GCCAGAGGGTAGGAGCTGTA-3'

PDL1 forward, 5'-ACATGTCAGGCTGAGGGCTA-3'

PDL1 reverse, 5'-TTGGTGGTGGTGGTCTTACC-3'

PDL2 forward, 5'-CAGTGGTTCGCGCCTAAAGC-3'
PDL2 reverse, 5'-GGTCCCTGGGTTCCATCTGAC-3'
IDO1 forward, 5'-CACTTTGCTAAAGGCGCTGT-3'
IDO1 reverse, 5'-CCCTTCATACACCAGACCGT-3'
IL10 forward, 5'-ATCAAGGCGCATGTGAACTC-3'
IL10 reverse, 5'-CATTCTTCACCTGCTCCACGG-3'

Immunoblotting

Protein lysates were electrophoresed by sodium dodecyl sulphate-polyacrylamide gel electrophoresis (SDS-PAGE) (10% gel) followed by iBlot transfer to polyvinylidene fluoride (Thermo Fisher Scientific). Membranes were blocked in 5% skim milk powder in TBS with 0.1% Tween-20 and then incubated overnight with primary antibody at 4 °C. The following primary antibodies were used: anti-PBK (PTG, 13739-1-AP), anti-CD276 (PTG, 14453-1-AP), anti-MSL1 (PTG, 24373-1-AP), anti- β -actin (PTG, 20536-1-AP), and anti-mouse and anti-rabbit peroxidase-conjugated secondary antibodies (CST, HAF007, and HAF008).

Co-immunoprecipitation and mass spectrometry analysis

For co-immunoprecipitation (co-IP), treated cells were lysed in IP lysis buffer (50 mM Tri-Cl (pH 7.4), 150 mM NaCl, 0.5% NP-40, and 5 mM EDTA) supplemented with PMSF (Sigma, USA) and protease inhibitor cocktail (Roche). The cell lysates were incubated with the indicated antibodies or Flag-beads (Sigma) overnight at 4 °C and washed with lysis buffer 4 times. Proteins were eluted and detected using immunoblotting assays with mouse antibody to Flag (Sigma, M2), an antibody to MSL1, and other appropriate antibodies.

For mass spectrometry analysis, 293T cells were transfected with Flag-PBK or vector control for 48 h. Then treated cells were lysed in IP lysis buffer (50 mM Tri-cl (pH 7.4), 150 mM NaCl, 0.5% NP-40, and 5 mM EDTA) supplemented with PMSF (Sigma, USA) and protease inhibitor cocktail (Roche) and incubated with Flag-tagged affinity agarose beads (Sigma, M2) overnight at 4 °C. The beads were then washed 4 times with IP lysis buffer. The immunoprecipitates were eluted and separated by SDS-PAGE and then stained via silver staining, and the indicated bands were subjected to mass spectrometry analysis.

qChIP assay

The ChIP assays were carried out with a ChIP assay kit (Upstate Biotechnology, Lake Placid, NY, USA) according to the manufacturer's instructions. The cultured NPC cells were fixed with 1% formaldehyde for 10 min at room temperature. Then, the ultrasonic breaker was set to 10 s per ultrasonic cycle with 10-s intervals with 15 cycles. Subsequently, the fragments underwent centrifugation (30,237 \times g) at 4 °C (part of the DNA fragments were used as input). The supernatant was collected and added with

IgG control (1 ug/ml) or indicated antibodies, including anti-MSL1 (1 ug/ml, Merckmillipore, ABE469), anti-MOF (1 μ g/ml, PTG, 13842-1-AP), and anti-H4K16ac (1 μ g/ml, CST, #13534), followed by incubation at 4 °C overnight. Protein Agarose/Sepharose was used to precipitate the endogenous DNA-protein complex. After a short period of centrifugation (1000 \times g), the supernatant was removed, and the nonspecific complex was washed. Following de-cross-linking at 65 °C overnight, DNA fragments were extracted, purified, and retrieved with phenol/chloroform. The enrichment of MSL1 or MOF or H4K16ac to *CD276* promoter region was detected via qPCR assay, and the specific primers of *CD276* promoter region were as follows:

5'-GGTGAATGCGCTTTTGCAGG-3'
 5'-CAGAGTGGACACGCCTAACC-3'

T-lymphocyte preparations

HLA-A2 expression of the T lymphocytes from healthy donors was screened via flow cytometry and only positive individuals subjected to leukapheresis collections. T lymphocytes were then isolated from peripheral blood lymphocytes by depletion of non-T lymphocytes using a Pan T Cell Isolation Kit (Cat# 130-096-535, Miltenyi Biotec). Isolated human T-lymphocyte cells were activated in a T-cell culture medium supplemented with Interleukin-2 (Cat# 200-02, Peprotech) in the pre-coated plate with anti-CD3 (Cat#300313, BioLegend) and anti-CD28 (Cat#302913, BioLegend).

T-cell killing assay

The prepared tumor cells and activated T cells were cocultured at a ratio of 1:40–1:1.25 (tumor:T cells) in triplicate and the cytolysis of tumor cells was evaluated using the xCELLingence real-time cell analysis system.

Data acquisition

Comprehensive immune cell abundance prediction is estimated via ImmuCellAI. The following RNA expression data of NPC samples were retrieved from GEO: GSE102349, GSE68799, GDS3341, GSE40290, and GSE53819.

Statistical analysis

All the experiments were conducted by three biological replicates with similar results. Student's *t* test was used to compare two independent groups of data. One-way analysis of variance was used to analyze the significance among multi groups. Pearson correlation analysis was performed as indicated. *P* value < 0.05 was considered statistically significant in all cases. Asterisk (*) means *P* < 0.05, asterisks (**) mean *P* < 0.01, and asterisks (***) mean *P* < 0.001. SEM means standard error of mean and SD means standard deviation. All statistical analyses were performed using the SPSS 16.0 or Graphpad 8.01.

Acknowledgements

This work was supported by grants from the National Natural Science Foundation of China (No. 81702690), from the Guangzhou Key Medical Discipline Construction Project fund, and from the Research Fund for the State key laboratory of oncology in south China (No. HN2017-09). We apologize to all colleagues whose work could not be cited due to space constraints. We thank Prof. Chao-Nan Qian for kindly providing NPC cancer cell lines.

Conflict of interest

The authors declare that they have no conflict of interest.

Publisher's note

Springer Nature remains neutral with regard to jurisdictional claims in published maps and institutional affiliations.

Supplementary Information accompanies this paper at (<https://doi.org/10.1038/s41389-020-00293-9>).

Received: 2 June 2020 Revised: 5 November 2020 Accepted: 30 November 2020

Published online: 05 January 2021

References

- Carioli, G. et al. Global trends in nasopharyngeal cancer mortality since 1970 and predictions for 2020: focus on low-risk areas. *Int. J. Cancer* **140**, 2256–2264 (2017).
- Ferlay, J. et al. Cancer incidence and mortality worldwide: sources, methods and major patterns in GLOBOCAN 2012. *Int. J. Cancer* **136**, E359–E386 (2015).
- Hui, E. P. et al. Lung metastasis alone in nasopharyngeal carcinoma: a relatively favorable prognostic group. A study by the Hong Kong Nasopharyngeal Carcinoma Study Group. *Cancer* **101**, 300–306 (2004).
- Hanahan, D. & Weinberg, R. A. Hallmarks of cancer: the next generation. *Cell* **144**, 646–674 (2011).
- Wenig, B. M. Lymphoepithelial-like carcinomas of the head and neck. *Semin. Diagn. Pathol.* **32**, 74–86 (2015).
- Chua, M. L. K., Wee, J. T. S., Hui, E. P. & Chan, A. T. C. Nasopharyngeal carcinoma. *Lancet* **387**, 1012–1024 (2016).
- Vaughan, T. L. et al. Nasopharyngeal cancer in a low-risk population: defining risk factors by histological type. *Cancer Epidemiol. Biomark. Prev.* **5**, 587–593 (1996).
- Minichsdorfer, C. et al. PD-L1 expression on tumor cells is associated with a poor outcome in a cohort of caucasian nasopharyngeal carcinoma patients. *Front. Oncol.* **9**, 1334 (2019).
- Hsu, C. et al. Safety and antitumor activity of pembrolizumab in patients with programmed death-ligand 1-positive nasopharyngeal carcinoma: results of the KEYNOTE-028 study. *J. Clin. Oncol.* **35**, 4050–4056 (2017).
- Fang, W. et al. Camrelizumab (SHR-1210) alone or in combination with gemcitabine plus cisplatin for nasopharyngeal carcinoma: results from two single-arm, phase 1 trials. *Lancet Oncol.* **19**, 1338–1350 (2018).
- Wang, L., Kang, F. B. & Shan, B. E. B7-H3-mediated tumor immunology: friend or foe? *Int. J. Cancer* **134**, 2764–2771 (2014).
- Chapoval, A. I. et al. B7-H3: a costimulatory molecule for T cell activation and IFN-gamma production. *Nat. Immunol.* **2**, 269–274 (2001).
- Sun, M. et al. Characterization of mouse and human B7-H3 genes. *J. Immunol.* **168**, 6294–6297 (2002).
- Hofmeyer, K. A., Ray, A. & Zang, X. The contrasting role of B7-H3. *Proc. Natl Acad. Sci. USA* **105**, 10277–10278 (2008).
- Seaman, S. et al. Eradication of tumors through simultaneous ablation of CD276/B7-H3-positive tumor cells and tumor vasculature. *Cancer Cell* **31**, 501–515 e508 (2017).
- Wu, C. P. et al. Relationship between co-stimulatory molecule B7-H3 expression and gastric carcinoma histology and prognosis. *World J. Gastroenterol.* **12**, 457–459 (2006).
- Altan, M. et al. B7-H3 expression in NSCLC and its association with B7-H4, PD-L1 and tumor-infiltrating lymphocytes. *Clin. Cancer Res.* **23**, 5202–5209 (2017).
- Zang, X. et al. B7-H3 and B7x are highly expressed in human prostate cancer and associated with disease spread and poor outcome. *Proc. Natl Acad. Sci. USA* **104**, 19458–19463 (2007).
- Li, M. et al. Overexpression of B7-H3 in CD14+ monocytes is associated with renal cell carcinoma progression. *Med. Oncol.* **31**, 349 (2014).
- Fauci, J. M., Straughn, J. M. Jr, Ferrone, S. & Buchsbaum, D. J. A review of B7-H3 and B7-H4 immune molecules and their role in ovarian cancer. *Gynecol. Oncol.* **127**, 420–425 (2012).
- Brunner, A., Hinterholzer, S., Riss, P., Heinze, G. & Brustmann, H. Immunoexpression of B7-H3 in endometrial cancer: relation to tumor T-cell infiltration and prognosis. *Gynecol. Oncol.* **124**, 105–111 (2012).
- Flem-Karlsen, K., Fodstad, O. & Nunes-Xavier, C. E. B7-H3 immune checkpoint protein in human cancer. *Curr. Med. Chem.* **27**, 4062–4086 (2020).
- Flem-Karlsen, K., Fodstad, O., Tan, M. & Nunes-Xavier, C. E. B7-H3 in cancer—beyond immune regulation. *Trends Cancer* **4**, 401–404 (2018).
- Tekle, C. et al. B7-H3 contributes to the metastatic capacity of melanoma cells by modulation of known metastasis-associated genes. *Int. J. Cancer* **130**, 2282–2290 (2012).
- Fauci, J. M. et al. Monoclonal antibody-based immunotherapy of ovarian cancer: targeting ovarian cancer cells with the B7-H3-specific mAb 376.96. *Gynecol. Oncol.* **132**, 203–210 (2014).
- Kasten, B. B. et al. B7-H3-targeted (212)Pb radioimmunotherapy of ovarian cancer in preclinical models. *Nucl. Med. Biol.* **47**, 23–30 (2017).
- Kramer, K. et al. Compartmental intrathecal radioimmunotherapy: results for treatment for metastatic CNS neuroblastoma. *J. Neurooncol.* **97**, 409–418 (2010).
- Loos, M., Hedderich, D. M., Friess, H. & Kleeff, J. B7-h3 and its role in antitumor immunity. *Clin. Dev. Immunol.* **2010**, 683875 (2010).
- Souweidane, M. M. et al. Convection-enhanced delivery for diffuse intrinsic pontine glioma: a single-centre, dose-escalation, phase 1 trial. *Lancet Oncol.* **19**, 1040–1050 (2018).
- Ahmed, M. et al. Humanized affinity-matured monoclonal antibody 8H9 has potent antitumor activity and binds to FG loop of tumor antigen B7-H3. *J. Biol. Chem.* **290**, 30018–30029 (2015).
- Loo, D. et al. Development of an Fc-enhanced anti-B7-H3 monoclonal antibody with potent antitumor activity. *Clin. Cancer Res.* **18**, 3834–3845 (2012).
- Aksamitiene, E., Kholodenko, B. N., Kolch, W., Hoek, J. B. & Kiyatkin, A. PI3K/Akt-sensitive MEK-independent compensatory circuit of ERK activation in ER-positive PI3K-mutant T47D breast cancer cells. *Cell Signal.* **22**, 1369–1378 (2010).
- Oh, S. M. et al. T-lymphokine-activated killer cell-originated protein kinase functions as a positive regulator of c-Jun-NH2-kinase 1 signaling and H-Ras-induced cell transformation. *Cancer Res.* **67**, 5186–5194 (2007).
- Roh, E. et al. Targeting PRP and TOPK for skin cancer prevention and therapy. *Oncogene* **37**, 5633–5647 (2018).
- Zykova, T. A. et al. T-LAK cell-originated protein kinase (TOPK) phosphorylation of Prx1 at Ser-32 prevents UVB-induced apoptosis in RPM17951 melanoma cells through the regulation of Prx1 peroxidase activity. *J. Biol. Chem.* **285**, 29138–29146 (2010).
- Herbert, K. J., Ashton, T. M., Prevo, R., Pirovano, G. & Higgins, G. S. T-LAK cell-originated protein kinase (TOPK): an emerging target for cancer-specific therapeutics. *Cell Death Dis.* **9**, 1089 (2018).
- Ishikawa, C., Senba, M. & Mori, N. Mitotic kinase PBK/TOPK as a therapeutic target for adult T cell leukemia/lymphoma. *Int. J. Oncol.* **53**, 801–814 (2018).
- Pirovano, G. et al. TOPK modulates tumour-specific radiosensitivity and correlates with recurrence after prostate radiotherapy. *Br. J. Cancer* **117**, 503–512 (2017).
- Wang, M. Y. et al. PDZ binding kinase (PBK) is a theranostic target for nasopharyngeal carcinoma: driving tumor growth via ROS signaling and correlating with patient survival. *Oncotarget* **7**, 26604–26616 (2016).
- Chang, C. F. et al. PBK/TOPK expression predicts prognosis in oral cancer. *Int. J. Mol. Sci.* **17**, 1007 (2016).
- Kim, D. J. et al. Novel TOPK inhibitor HI-TOPK-032 effectively suppresses colon cancer growth. *Cancer Res.* **72**, 3060–3068 (2012).
- Matsuo, Y. et al. TOPK inhibitor induces complete tumor regression in xenograft models of human cancer through inhibition of cytokinesis. *Sci. Transl. Med.* **6**, 259ra145 (2014).
- Gao, G. et al. ADA-07 suppresses solar ultraviolet-induced skin carcinogenesis by directly inhibiting TOPK. *Mol. Cancer Ther.* **16**, 1843–1854 (2017).
- Azimi, F. et al. Tumor-infiltrating lymphocyte grade is an independent predictor of sentinel lymph node status and survival in patients with cutaneous melanoma. *J. Clin. Oncol.* **30**, 2678–2683 (2012).
- Miao, Y. R. et al. ImmuCellAI: a unique method for comprehensive T-cell subsets abundance prediction and its application in cancer immunotherapy. *Adv. Sci.* **7**, 1902880 (2020).

46. Szczerba, B. M. et al. Neutrophils escort circulating tumour cells to enable cell cycle progression. *Nature* **566**, 553–557 (2019).
47. Coffelt, S. B., Wellenstein, M. D. & de Visser, K. E. Neutrophils in cancer: neutral no more. *Nat. Rev. Cancer* **16**, 431–446 (2016).
48. Olingy, C. E., Dinh, H. Q. & Hedrick, C. C. Monocyte heterogeneity and functions in cancer. *J. Leukoc. Biol.* **106**, 309–322 (2019).
49. Hodgins, J. J., Khan, S. T., Park, M. M., Auer, R. C. & Ardolino, M. Killers 2.0: NK cell therapies at the forefront of cancer control. *J. Clin. Investig.* **129**, 3499–3510 (2019).
50. Guillerrey, C., Huntington, N. D. & Smyth, M. J. Targeting natural killer cells in cancer immunotherapy. *Nat. Immunol.* **17**, 1025–1036 (2016).
51. Ding, T., Yan, F., Cao, S. & Ren, X. Regulatory B cell: new member of immunosuppressive cell club. *Hum. Immunol.* **76**, 615–621 (2015).
52. Kochenderfer, J. N. et al. Chemotherapy-refractory diffuse large B-cell lymphoma and indolent B-cell malignancies can be effectively treated with autologous T cells expressing an anti-CD19 chimeric antigen receptor. *J. Clin. Oncol.* **33**, 540–549 (2015).
53. Luckheeram, R. V., Zhou, R., Verma, A. D. & Xia, B. CD4(+)T cells: differentiation and functions. *Clin. Dev. Immunol.* **2012**, 925135 (2012).
54. Kamphorst, A. O. et al. Proliferation of PD-1+ CD8 T cells in peripheral blood after PD-1-targeted therapy in lung cancer patients. *Proc. Natl Acad. Sci. USA* **114**, 4993–4998 (2017).
55. Vinay, D. S. et al. Immune evasion in cancer: mechanistic basis and therapeutic strategies. *Semin. Cancer Biol.* **35**, S185–S198 (2015).
56. Beatty, G. L. & Gladney, W. L. Immune escape mechanisms as a guide for cancer immunotherapy. *Clin. Cancer Res.* **21**, 687–692 (2015).
57. Wilky, B. A. Immune checkpoint inhibitors: the linchpins of modern immunotherapy. *Immunol. Rev.* **290**, 6–23 (2019).
58. Alachkar, H. et al. T-LAK cell-originated protein kinase presents a novel therapeutic target in FLT3-ITD mutated acute myeloid leukemia. *Oncotarget* **6**, 33410–33425 (2015).
59. Ikeda, Y. et al. T-LAK cell-originated protein kinase (TOPK) as a prognostic factor and a potential therapeutic target in ovarian cancer. *Clin. Cancer Res.* **22**, 6110–6117 (2016).
60. Zhou, H. et al. Toward a comprehensive characterization of a human cancer cell phosphoproteome. *J. Proteome Res.* **12**, 260–271 (2013).
61. Bian, Y. et al. An enzyme assisted RP-RPLC approach for in-depth analysis of human liver phosphoproteome. *J. Proteom.* **96**, 253–262 (2014).
62. Smith, E. R. et al. A human protein complex homologous to the Drosophila MSL complex is responsible for the majority of histone H4 acetylation at lysine 16. *Mol. Cell Biol.* **25**, 9175–9188 (2005).
63. Conrad, T. & Akhtar, A. Dosage compensation in *Drosophila melanogaster*: epigenetic fine-tuning of chromosome-wide transcription. *Nat. Rev. Genet.* **13**, 123–134 (2012).
64. Chelminski, T. et al. MOF-associated complexes ensure stem cell identity and Xist repression. *Elife* **3**, e02024 (2014).
65. Li, X. et al. The histone acetyltransferase MOF is a key regulator of the embryonic stem cell core transcriptional network. *Cell Stem Cell* **11**, 163–178 (2012).
66. Ravens, S. et al. Mof-associated complexes have overlapping and unique roles in regulating pluripotency in embryonic stem cells and during differentiation. *Elife* **3**, e02104 (2014).
67. Deng, X. et al. Mammalian X upregulation is associated with enhanced transcription initiation, RNA half-life, and MOF-mediated H4K16 acetylation. *Dev. Cell* **25**, 55–68 (2013).
68. Bao, Y. N. et al. Urokinase-type plasminogen activator receptor signaling is critical in nasopharyngeal carcinoma cell growth and metastasis. *Cell Cycle* **13**, 1958–1969 (2014).
69. Suh, W. K. et al. The B7 family member B7-H3 preferentially down-regulates T helper type 1-mediated immune responses. *Nat. Immunol.* **4**, 899–906 (2003).
70. Prasad, D. V. et al. Murine B7-H3 is a negative regulator of T cells. *J. Immunol.* **173**, 2500–2506 (2004).
71. Zhu, F. et al. Bidirectional signals transduced by TOPK-ERK interaction increase tumorigenesis of HCT116 colorectal cancer cells. *Gastroenterology* **133**, 219–231 (2007).
72. Roh, E. et al. Suppression of the solar ultraviolet-induced skin carcinogenesis by TOPK inhibitor HI-TOPK-032. *Oncogene* **39**, 4170–4182 (2020).
73. Liu, K. et al. Sunlight UV-induced skin cancer relies upon activation of the p38alpha signaling pathway. *Cancer Res.* **73**, 2181–2188 (2013).
74. Zykova, T. A. et al. The T-LAK cell-originated protein kinase signal pathway promotes colorectal cancer metastasis. *EBioMedicine* **18**, 73–82 (2017).
75. Lu, H. et al. TOPK inhibits autophagy by phosphorylating ULK1 and promotes glioma resistance to TMZ. *Cell Death Dis.* **10**, 583 (2019).
76. Zhao, J. et al. MicroRNA-187, down-regulated in clear cell renal cell carcinoma and associated with lower survival, inhibits cell growth and migration through targeting B7-H3. *Biochem. Biophys. Res. Commun.* **438**, 439–444 (2013).
77. Nygren, M. K. et al. Identifying microRNAs regulating B7-H3 in breast cancer: the clinical impact of microRNA-29c. *Br. J. Cancer* **110**, 2072–2080 (2014).